J Nanopart Res (2022) 24:251
https://doi.org/10.1007/s11051-022-05633-x

RESEARCH PAPER

Preparation of nano-ZrB_2 powder by Ca liquid assisted boronation reaction between ZrC and B_4C

Yu Wang · Yao Li · Xiao-Hui Yang · Guo-Hua Zhang

Received: 15 September 2022 / Accepted: 21 November 2022 / Published online: 29 November 2022
© The Author(s), under exclusive licence to Springer Nature B.V. 2022

Abstract Nano-Zirconium diboride (ZrB_2) powder was vital raw material for manufacturing ultra-high temperature ceramics (UHTCs) and C/C composite materials, which were widely used in extreme environment. In this paper, a convenient way of synthesizing nano-ZrB_2 powder was proposed. Firstly, the precursor consisting of ultrafine-ZrC and C was obtained via vacuum carbothermal reduction of nano-ZrO_2. And then, the carbothermal reduction product was boronized by B_4C in Ca melt. In boronation process, Ca melt would play a key role as decarburizer. By boronation reaction at 1373 K and 1473 K, cauliflower-shaped ZrB_2 particle and smooth polyhedral ZrB_2 particle were obtained, respectively. XRD and BET analyses showed that the grain sizes and BET-equivalent particle diameters of these two products were less than 100 nm.

Keywords Borides · Grain size · Decarbonization in Ca melt · Ultra-high-temperature ceramics · Nanostructures

Y. Wang · Y. Li · X.-H. Yang · G.-H. Zhang (✉)
State Key Laboratory of Advanced Metallurgy, University of Science and Technology, Beijing, Beijing 100083, China
e-mail: ghzhang_ustb@163.com; ghzhang0914@ustb.edu.cn

Y. Wang · Y. Li · X.-H. Yang · G.-H. Zhang
Beijing Key Laboratory of Green Recovery and Extraction of Rare and Precious Metals, University of Science and Technology, Beijing, Beijing 100083, China

Introduction

The characteristics such as extreme melting point (3245 ℃), high hardness, and well oxidation resistance make ZrB_2 a superior material used in the extreme environment [1]. ZrB_2-based ceramics and ZrB_2-containing C/C composite materials are expected to find wide application in thermal shield materials for rockets and hypersonic vehicle [2, 3]. Since nano-ZrB_2 powder has a higher sintering activity, the sintering temperature would be significantly decreased if coarse raw material is replaced with nano powder [4]. In addition, using nano-powder as raw material is an important way of reducing grain size of sintered products, and thus improve their strength and hardness [5, 6]. Moreover, manufacture of ZrB_2-containing C/C composite materials needs homogeneous ZrB_2 slurry for coating and impregnating, and nano-ZrB_2 powder is vital raw material for obtaining homogeneous ZrB_2 slurry [7, 8]. Therefore, synthesizing nano-ZrB_2 powder is crucially important for developing ZrB_2-based materials.

Lots of methods had been provided to synthesize nano-ZrB_2 powder. By mechanochemical processing and subsequent annealing, Guo et al. [9] obtained nano-ZrB_2 with grain size of 5–40 nm using the raw materials of ZrH_2 and amorphous boron. In work of Wu et al. [10], nanocrystalline ZrB_2 (10 ~ 14 nm) was prepared via mechanical alloying using Zr and B. Based on mechanically induced self-sustaining reaction (MSR) among ZrO_2, B_2O_3, and Mg, Jalaly et al. [11]

and Yuan et al. [12] manufactured nano-ZrB_2 powder with size of 56 and 50 nm, respectively. Bai et al. [13] synthesized ultra-fine ZrB_2 powders (100 nm) by RF thermal plasma-assisted metallothermic reduction reaction. In work of Zoli et al. [14], ZrB_2 with size of 100 nm was obtained by reaction between ZrO_2 and $NaBH_4$ at 900 ℃. Camurlu and Maglia [15] studied preparation of nano-sized ZrB_2 powder by self-propagation high-temperature synthesis (SHS), and the finest ZrB_2 product reached 32 nm. In order to compare these methods, the characteristics of these methods are listed in Table 1. High-value raw materials (such as metallic Zr, amorphous B, and borohydride), special equipment, or strong reaction heats made those methods are not suitable for industrial production. Therefore, even if many different methods had been proposed, it was still a challenge to produce nano-ZrB_2 powder via a simple, efficient, and low-cost pathway. In our previous work [16, 17], a universal method for the synthesis of refractory metal diborides had been proposed. In addition, the inheritance relationship of particle size among raw oxide, intermediate carbide, and finally prepared diboride was revealed. In this method, readily-accessible materials (ZrO_2, C, B_4C, and Ca) were used, which would ensure a low overall cost. These characteristics make nano-ZrB_2 expected to be synthesized in mass production at a low price.

In order to avoid the direct reaction between B_4C and oxides which could lead to the vaporization loss of boron, the high-temperature process was divided into two steps, achieving the accurate batching of boron source. In the first step, the carbothermal reduction of ZrO_2 (Eq. (1)) was taken place to remove the oxygen and generate ZrC. In the second step, ZrC was boronized by B_4C (Eq. (2)), and Ca would react with residual carbon to form CaC_2 (Eq. (3)). Reaction enthalpy and adiabatic temperature of each reaction showed that the carbothermal reduction reaction was endothermic, while the boronation and decarburization reactions were not violent exothermic reactions. Therefore, this method was expected to be operated in large batches. In Fig. 1, The changes of Gibbs free energy (ΔG^{Θ}) for these reactions were calculated, which indicated that these reactions would spontaneously occur in a wide temperature range.

$$\begin{gathered} ZrO_2 + 3C = ZrC + 2CO(g) \\ \Delta H_{298} > +680\text{kJ} \bullet \text{mol}^{-1} \end{gathered} \tag{1}$$

$$\begin{gathered} ZrC + 0.5B_4C = ZrB_2 + 1.5C \\ \Delta H_{298} = -95\text{kJ} \bullet \text{mol}^{-1} T_{ad298} = 1291\text{K} \end{gathered} \tag{2}$$

Table 1 Several preparation methods of nano-ZrB_2

Ref	Raw material	Reaction condition	Phase of product	Particular size/nm	Features
[9]	ZrH_2, amorphous B	Ball milling and self-propagating reaction	ZrB_2, ZrO_2	24.87	Simple reaction process Impure product Expensive amorphous B Special equipment
[10]	ZrH_2, amorphous B	Ball milling	ZrB_2	10	Simple reaction process Expensive amorphous B Special equipment
[11]	ZrO_2, Mg, B_2O_3	Ball milling and leaching	ZrB_2	56	Cheap raw materials Strong heat release Special equipment
[12]	ZrO_2, Mg, B_2O_3	Ball milling and leaching	ZrB_2	200–400	Cheap raw materials Strong heat release Special equipment
[13]	$ZrCl_4$, Mg, amorphous B	RF thermal plasma system and leaching	ZrB_2	100	Special equipment
[14]	ZrO_2, $NaBH_4$	1173 ~ 1373 K	ZrB_2	100	Simple reaction process Expensive $NaBH_4$
[15]	Zr, amorphous B, NaCl	Igniting and leaching	ZrB_2	32	Simple reaction process Strong heat release Expensive amorphous B

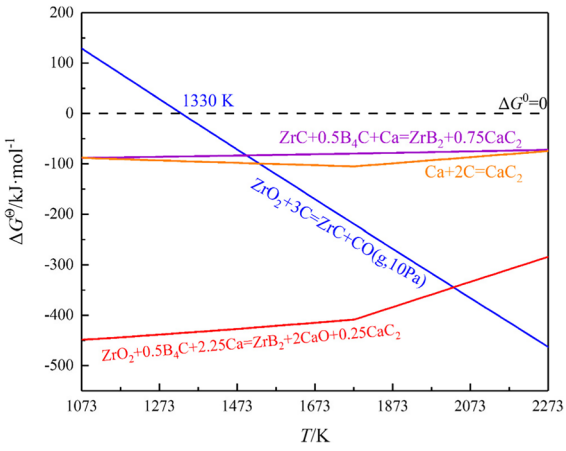

Fig. 1 Changes of the standard Gibbs free energy of related reactions

$$2C + Ca = CaC_2$$
$$\Delta H_{298} = -60\text{kJ} \bullet \text{mol}^{-1} T_{\text{ad}298} = 1059\text{K} \quad (3)$$

For removing by-product CaC_2 and residual Ca, the product was soaked in hydrochloric acid. Our previous findings suggested that there may be an inheritance rule in particle sizes of final boride products and raw oxides. According to the above analysis, this method might use cheap raw materials to prepare nano-ZrB_2 powder through a mild reaction process. Therefore, in order to synthesize nano-ZrB_2, nano-ZrO_2 was used in this work. This article would focus on the effects of various parameters (proportion of carbon black, boronizing temperature, and proportion of Ca) on particle size and microstructure of ZrB_2 powder products.

Experimental procedure

In this work, the used raw materials were nano-ZrO_2 powder (purity > 99%, Shanghai Macklin Biochemical Co., Ltd., Shanghai, China), carbon black powder (purity > 98.5%, Mitsubishi Chemical Corporation, Tokyo, Japan), B_4C powder (purity > 98%, 2 ~ 10 μm Shanghai Aladdin Bio-Chem Technology Co. Ltd.), and Ca particles (purity > 99.5%, 1–5 mm, Beijing Universal Jin Xin International Science and Technology Co., LTD, Beijing, China). Micromorphologies of raw powders are displayed in Fig. 2. Among them, sizes of spherical nano-ZrO_2 and carbon black particles are 30 ~ 100 nm and ~ 50 nm, respectively, while B_4C has polyhedron particle with size of several microns.

Considering the main gaseous product is CO, according to stoichiometric ratio of Eq. (1), three proportions of carbon black ($C/ZrO_2 = 0.8$, 1.0, 1.2) were selected, which represented the conditions of deficient, theoretical, and excess carbon addition, respectively. Firstly, nano-ZrO_2 and carbon black with different proportions were weighed and homogeneously mixed in a slurry state by adding absolute ethyl alcohol in an agate mortar. Next, slurry was dried and subjected to carbothermal reduction. In order to obtain as fine ZrC particles as possible, vacuum condition (10 Pa) was adopted to reduce the carbothermal reduction temperature. The reaction was carried out in a tube furnace at 1773 K. According to Reaction (2), the B_4C powder was weighed according to a Zr/B_4C molar ratio of 0.5. The obtained carbothermal reduction precursor was mixed with B_4C powder, and then Ca particles were added to the mixture powder. Boronation reaction was performed in a graphite crucible. For the investigations of boronation stage, including the influences of boronizing temperature (1273, 1373, and 1473 K) and mass ratio of Ca to carbothermal reduction product, the sample with a carbon proportion of 1.2 was used for all experiments. All experimental parameters are listed in Table 2. After boronation reaction, the sample was immersed in dilute hydrochloric acid (~ 9 wt.%) for 1 h. The remaining solid was washed with deionized water, and dried powder was collected for characterization.

The phases of samples were detected using powder X-ray diffraction analysis (XRD, SMARTLAB (9), Japan, Cu-Kα radiation, λ = 1.54178 Å) in a 2θ range of 20 ~ 80° with a scanning rate of $30°\cdot\text{min}^{-1}$. The micromorphology of powders was obtained using a field-emission scanning electron microscope (FE-SEM, (FE-SEM, Gemini SEM500, ZEISS, Germany). The C content was analyzed using a carbon–sulfur analyzer (EMIA—920V2, HORIBA). The O content was analyzed using an oxygen–nitrogen-hydrogen analyzer (EMGA—830, HORIBA). The changes of Gibbs free energy of reactions were calculated using thermodynamic software Fact-Sage 7.0. The surface area was determined by Brunauer–Emmett–Teller method (ASAP 2460, Micromeritics, USA).

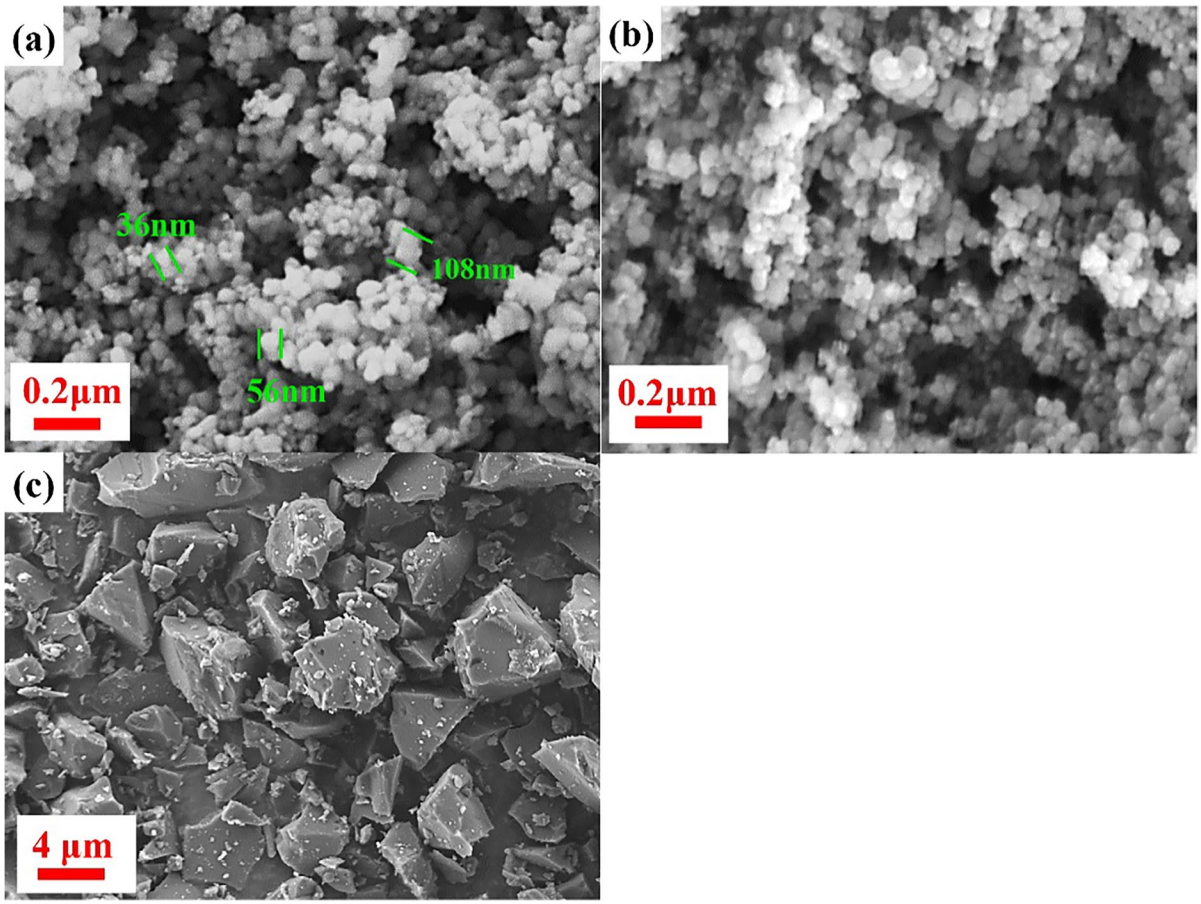

Fig. 2 FE-SEM images of raw material powders: **a** nano-ZrO_2; **b** carbon black; **c** B_4C

Table 2 Experimental parameters of study

No	Carbothermal reduction stage		Boronation stage	
	Carbon proportion	Temperature schedule	Mass ratio of Ca to carbothermal reduction product	Temperature schedule
1	0.8	1773 K, 4 h	1.0	1373 K, 4 h
2	1.0		1.0	
3	1.2		1.0	
4			1.0	1273 K, 4 h
5			1.0	1473 K, 4 h
6			0.5	1373 K, 4 h
7			2.0	

Results and discussion

Influence of carbon proportion on boronized product

In Fig. 3a, the XRD patterns of carbothermal products with different carbon proportions are displayed. The relative intensities of ZrO_2 decrease in reduced products, as gradually increasing carbon proportion. However, even though the amount of reducing agent is sufficient for sample with a carbon proportion of

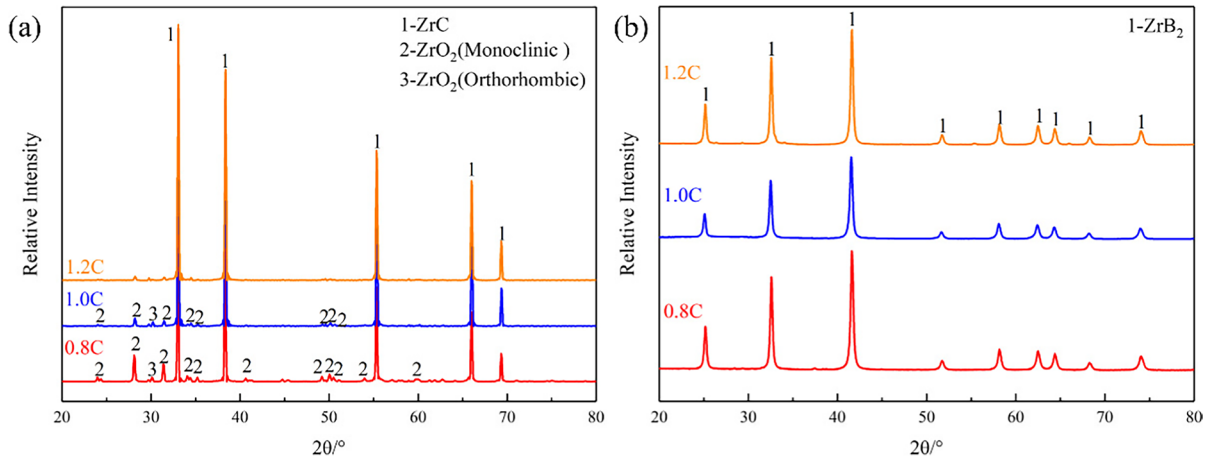

Fig. 3 XRD patterns of **a** carbothermal reduction products and **b** boronized products

1.0, there is still a small amount of unreduced ZrO_2. This phenomenon might be due to that the remaining ZrO_2 and carbon black were isolated by the formed ZrC particles. So, the excess carbon addition (such as 1.2) could obviously facilitate the reduction of ZrO_2. As shown in Fig. 3a, there are not too much ZrO_2 remaining in the product. After boronizing by B_4C in Ca melt, all boronized products were pure ZrB_2, as shown in Fig. 3b. It was worth noting that the precursor containing unreacted ZrO_2 was also fully transformed to ZrB_2. This result indicated that ZrO_2 could also be reduced by Ca and then boronized by B_4C, as described by Eq. (4). The thermodynamic calculation (Fig. 1) reveals that this process can occur spontaneously.

$$ZrO_2 + 0.5B_4C + 2.25Ca = ZrB_2 + 2CaO + 0.25CaC_2$$
$$\Delta H = -478.9\text{kJ} \bullet \text{mol}^{-1} \quad T_{ad298} = 2663\text{K} \tag{4}$$

The phase analysis results showed that carbon proportions had no effect upon the phase composition of final boronized product.

In order to study the morphological regularity of the carbothermal reduction products, the micromorphologies of products with different carbon proportions are shown in Fig. 4. In sample with a carbon proportion of 0.8 (Fig. 4a), two type particles with sizes of ~ 1 μm and ~ 200 nm are observed. EDS analysis shows stronger O signal in the region of large particles. Combining with the XRD diffraction results, these large particles were identified as ZrO_2 and the small particles were confirmed as ZrC. Compared with the raw nano-ZrO_2, the size of these residual ZrO_2 increased by a dozen times. This phenomenon was due to the fact that nano-ZrO_2 could be easily sintered at 1223 ~ 1473 K [18, 19]. When the carbon proportion is 0.8, the carbothermal reduction products would contain a large amount of un-reduced ZrO_2, and these nano-ZrO_2 particles would be sintered to bigger particles. However, sintering of ZrC needed a high temperature of above 2000 K [20, 21], which indicated that ZrC particles would not continue to grow up in the current conditions. Therefore, ultrafine-ZrC particles would be remained in products. In products with carbon proportions of 1.0 and 1.2 (Fig. 4 b and c), large ZrO_2 particles are no longer observed, and the sizes of obtained ZrC particles were also ~ 200 nm. Especially for the case with a carbon proportion of 1.2, ultrafine particles of excess carbon black can still be found around the ZrC particles.

Next, carbothermal reduction products with different carbon proportions (0.8, 1.0, and 1.2) were boronized. After leaching and drying, the corresponding FE-SEM images of products are shown in Fig. 5. Phase analyses had shown that these products were all pure ZrB_2. For boronation product with a carbon proportion of 0.8 (Fig. 5 a and b), two types of particles with different sizes are also observed and are similar to carbothermal reduction products, since original sizes of both ZrC and ZrO_2 particles were inherited to ZrB_2 formed during boronizing process. Both two types of ZrB_2 particles are not smooth. The small

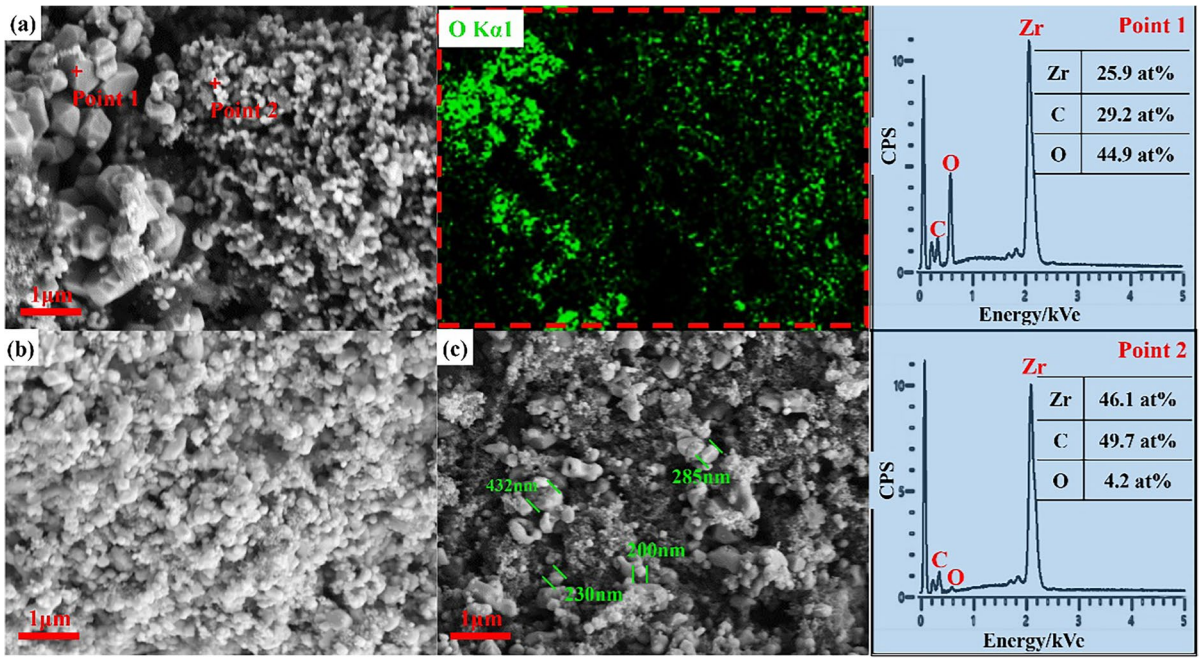

Fig. 4 FE-SEM images of carbothermal reduction products obtained with a carbon proportion of **a** 0.8, **b** 1.0, and **c** 1.2

particles are cauliflower-like, while the large particles are porous. The formation of ZrB_2 with cauliflower-like morphology was resulted from boronization of ZrC. In this process, the molar volume becomes larger from 15.47 (ZrC) to 18.49 $cm^3 \cdot mol^{-1}$ (ZrB_2), as shown in Table 3. Originally smooth ZrC particles transformed into non-smooth ZrB_2 due to volume expansion and the resulting stress. But the transformation from ZrO_2 to ZrB_2 was a process of reducing molar volume (from 21.2 to 15.47 $cm^3 \cdot mol^{-1}$), so the porous large ZrB_2 particle was the result of volume shrinkage. For boronation products with carbon proportions of 1.0 and 1.2, there are only cauliflower-like ZrB_2 particles with size of 200 nm in the view. Through the above analysis, it can be seen that the excess C addition could ensure that there are no lager ZrO_2 particles in carbothermal reduction product, which would make the final boronized product fine and homogeneous.

Influence of boriding temperature on boronized product

In order to obtain finer ZrB_2 powder, carbothermal reduction product with a carbon proportion of 1.2 was used for further researches. Boronation experiments at different temperatures were performed, and the XRD patterns of the products are shown in Fig. 6. After boronizing the sample at 1273 K for 4 h, there are ZrC, ZrB_2, and CaB_2C_2 in product. The characteristic peak of ZrC is the highest in XRD spectrum of product, and it can be concluded that the boronation reaction of ZrC was weak at such a low temperature (1273 K). In addition, B_4C could react with Ca to form CaB_2C_2, and this phenomenon had also been verified in the process of preparing CaB_6 with Ca and B_4C as raw materials [22]. As the temperature is increased to 1373 and 1473 K, the boronized product is pure ZrB_2.

The micromorphology of boronation products obtained at 1373, 1273, and 1473 K are displayed in Figs. 5d and 7 a and b, respectively. For products prepared at 1273 K, there are many ultra-fine particles and a small number of large particles in the view. The EDS analysis (point 1) show that B and Ca elements are enriched in region of bigger particle, from which it could be speculated that the large particles are CaB_2C_2. In high magnification view, cauliflower-like particles and smooth particles are found, both of which are about 200 nm. Moreover,

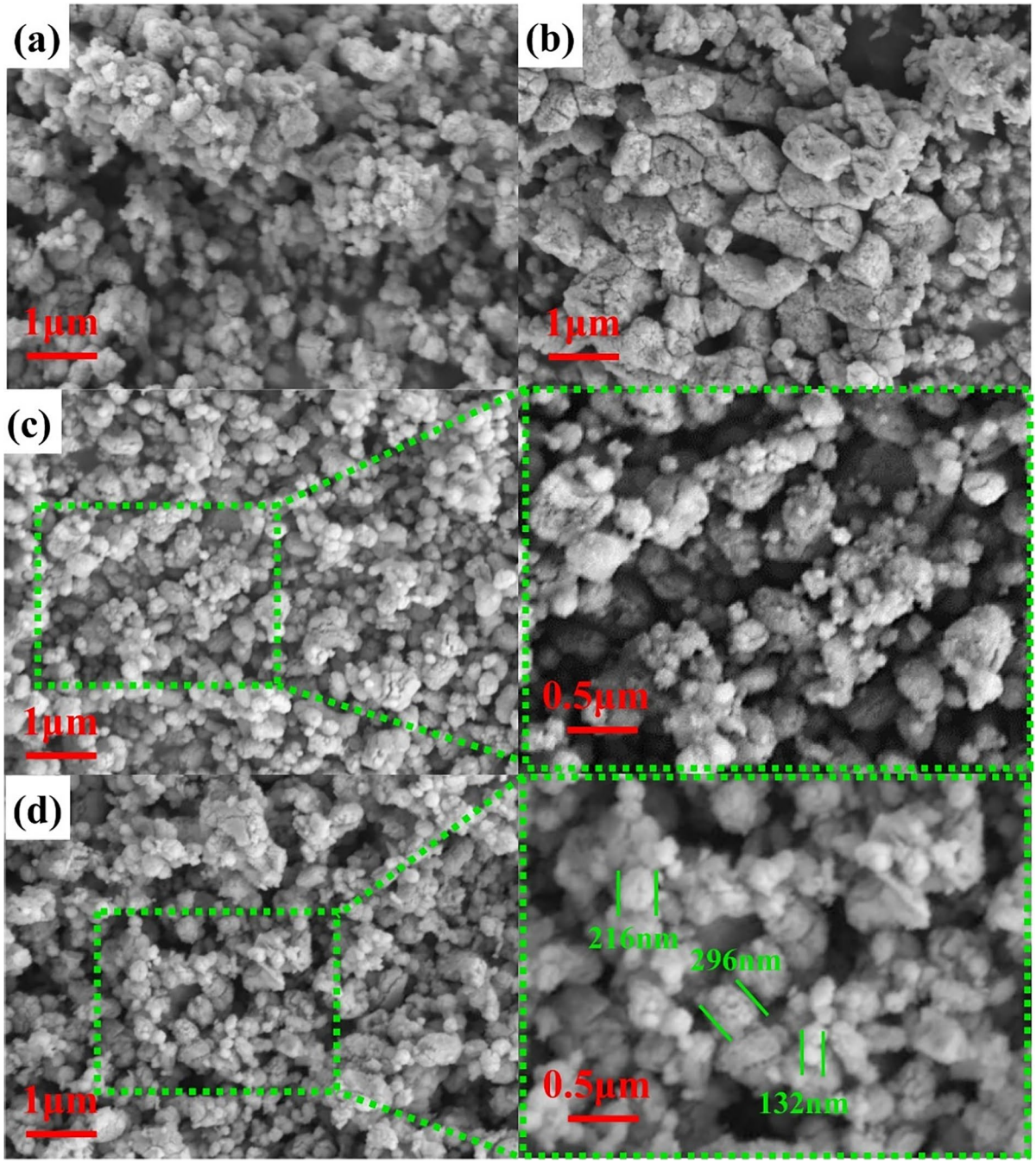

Fig. 5 FE-SEM images of boronized products with carbon proportion of **a** and **b** 0.8, **c** 1.0, **d** 1.2

EDS analysis (points 2 and 3) indicated that cauliflower-like and smooth particles are ZrB_2 and unreacted ZrC, respectively. This finding was consistent with the above analysis. For products prepared at 1373 K (Fig. 5d), there were all cauliflower-like particles with size of ~ 200 nm. However, the morphology of ZrB_2 prepared at 1473 K is significantly different from that obtained at lower temperatures. Most of ZrB_2 particles are smooth polyhedrons with the sizes of less than 100 nm. Compared with low

Table 3 Physical parameters of related compounds

Compound	ZrO_2	ZrC	ZrB_2
Density/g·cm^{-3}	5.813	6.675	6.104
Molar mass/g·mol^{-1}	123.22	103.23	112.84
Molar volume/cm^3·mol^{-1}	21.20	15.47	18.49

temperature product, the dispersity of product is significantly improved. In addition, nano-carbon particles cannot be observed in all boronized products, which means that excess carbon black were removed by Ca melt (Reaction (3)). Therefore, the boriding temperature was an important factor affecting the rate

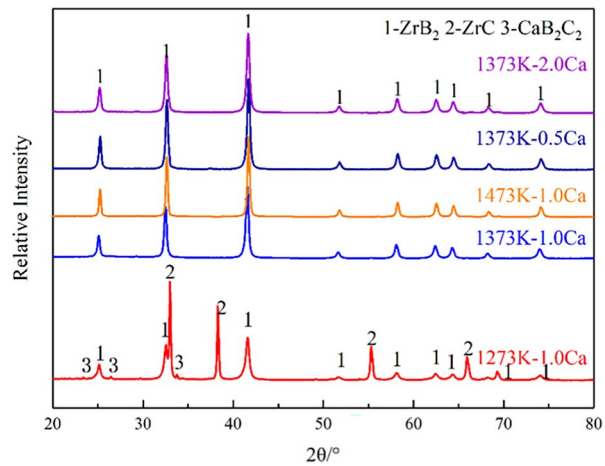

Fig. 6 XRD patterns of boronized products with different conditions

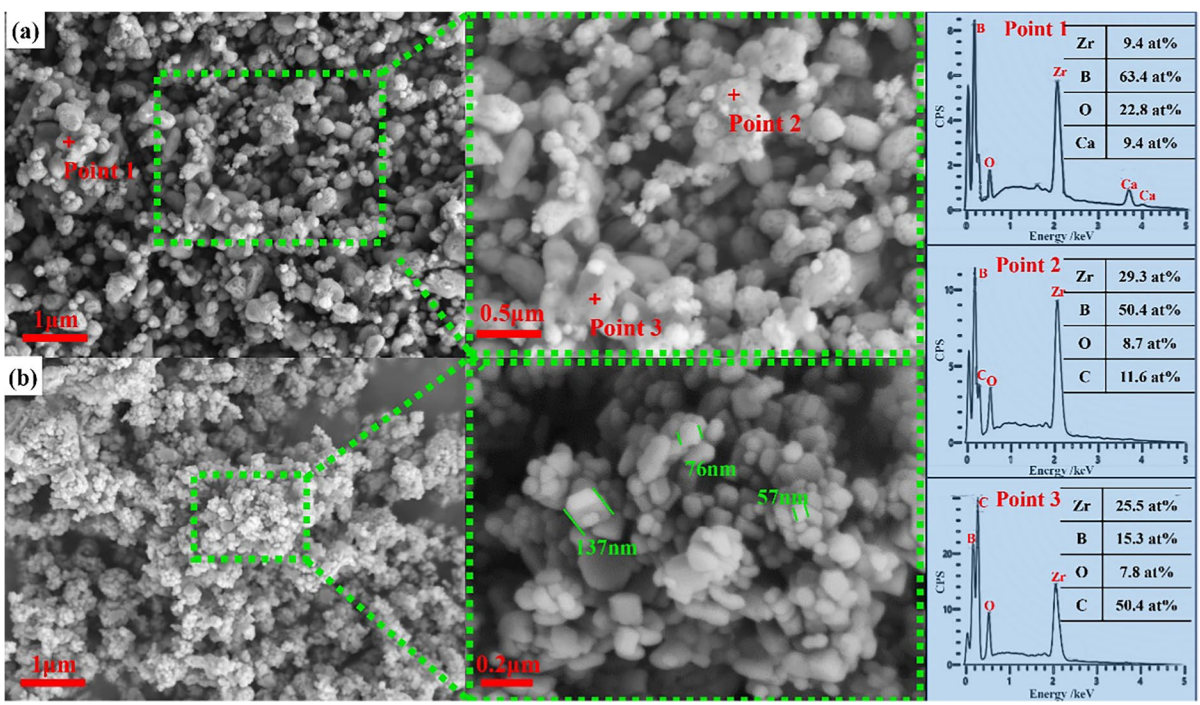

Fig. 7 FE-SEM images of boronized products with different temperatures: **a** 1273 K, **b** 1473 K

of boronation process and microstructure of produced ZrB_2.

Influence of Ca proportion on boronized product

To compare the effect of Ca addition amount on the boronation process, experiments with different Ca mass ratios were also carried out at 1373 K. Phase analysis shows that the composition of these products is single phase ZrB_2, as shown in Fig. 6. FE-SEM images of products with Ca proportions of 1.0, 0.5, and 2.0 are shown in Figs. 5d and 8 a and b, respectively. Since these products were prepared at 1373 K, all of them are cauliflower-like particles with size of ~ 200 nm. In addition, it could be concluded that the Ca proportion had no significant effect on boronized products.

Assessment of nano-ZrB_2

In order to compare the difference of ZrB_2 powders prepared at two temperatures (1373 and 1473 K), some relevant parameters are listed in Table 4. Firstly, full width at half maximum (FWHM) was used for calculating grain size by Scherrer's formula (Eq. (5)) [23, 24] (where Dc is calculational grain size; λ is the X-ray wavelength, 0.154178 nm; θ is the diffraction angle).

$$D_C = \frac{0.89\lambda}{\mathrm{FWHM}\cos\theta} \tag{5}$$

Obviously, the D_C value (49 nm) was smaller than the size (about 200 nm) of the cauliflower-like particles observed in Fig. 5d. This phenomenon indicated that the cauliflower-like ZrB_2 were not single crystal particles, and were aggregates

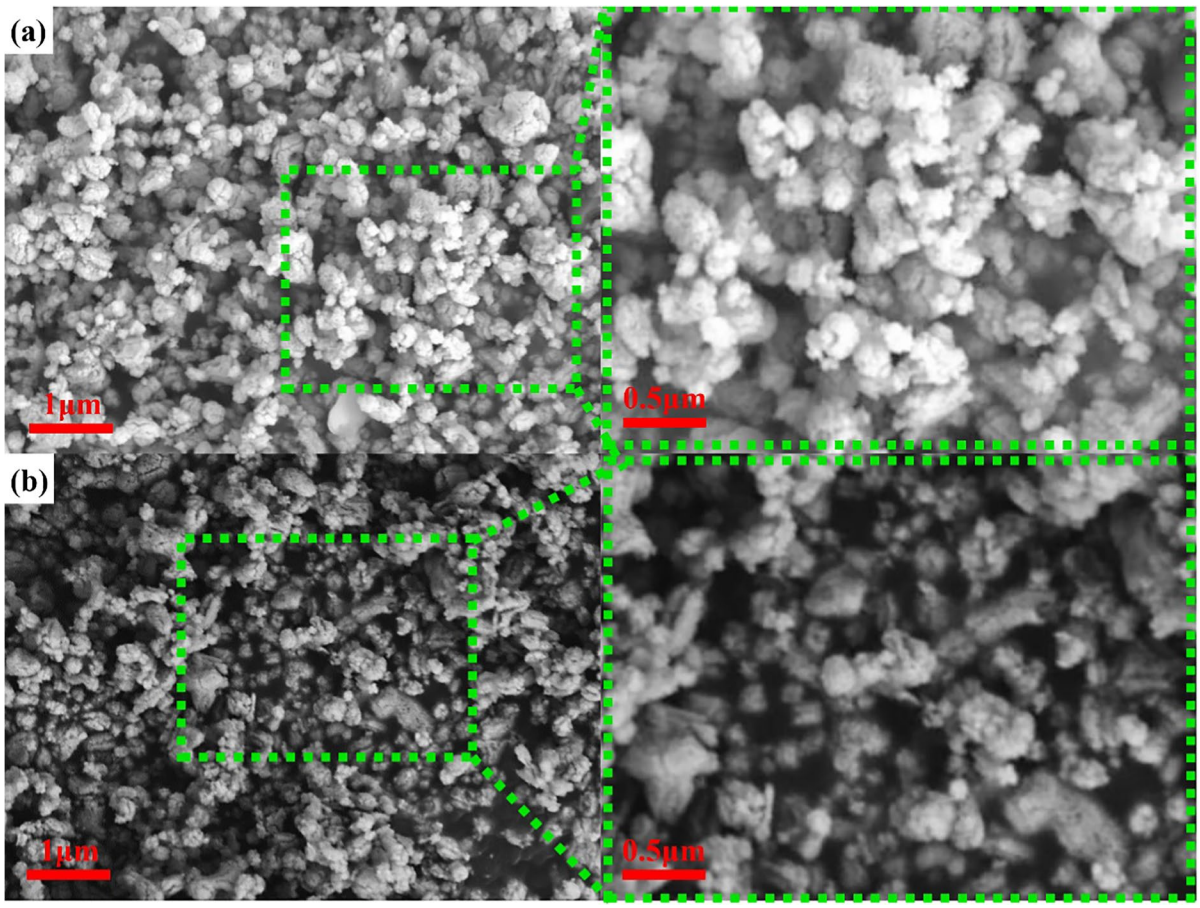

Fig. 8 FE-SEM images of boronized products obtained with different Ca proportions: **a** 0.5, **b** 2.0

Table 4 Relevant parameters of ZrB_2 powders prepared at two temperatures

Temp./K	Micromorphology	FWHM of [001] peak/Rad	D_C/nm	S_g/m^2·g^{-1}	D_E/nm	Carbon content/wt.%	Oxygen content/wt.%	S_O/g·m^{-2}	d/nm
1373	Cauliflower-like particle	2.85×10^{-3}	49	16.65	59.1	0.69	2.53	1.52×10^{-3}	1.16
1473	Smooth polyhedron	1.68×10^{-3}	84	10.74	89.9	0.64	1.57	1.46×10^{-3}	1.05

FWHM full width at half maximum, D_C calculational grain size by Scherrer's formula, S_g specific surface area, D_E equivalent particle size according to specific surface area, S_O oxygen content per unit surface, d thickness of surface oxide layer

composed of many nano particles. In addition, according to Eq. (6) [9] (where D_E is equivalent particle size; S_g is specific surface area and ρ is density of ZrB_2, 6.104 g·cm^{-3}), the equivalent particle size was estimated by using the specific surface area.

$$D_E = \frac{6}{S_g \rho} \tag{6}$$

D_E of cauliflower-like particles is 59.1 nm and is similar to value of D_C calculated by Eq. (5). For product obtained at 1473 K, D_C (84 nm) is larger than that (49 nm) prepared at 1373 K. However, this value was roughly equivalent to the particle size observed by FE-SEM (Fig. 7b), which meant that smooth polyhedron might be single crystal particle. In addition, the corresponding D_E is 89.9 nm, which is also near the value of D_C. For boronation reaction at 1473 K, it was speculated that the original cauliflower-like agglomerates ($D_C = 49$ nm) grew into smooth polyhedron ($D_C = 84$ nm) at high temperature. During growing process of cauliflower-like agglomerates, several small grains were combined to form a ZrB_2 particle with size of about 100 nm. Meanwhile, the original agglomerates were disintegrated due to grain growth, and the dispersity of the particles was also improved.

To further assess the purities of two samples, C and O contents of two samples were also tested. The carbon contents of two samples are similar, as shown in Table 4. However, the O content of cauliflower-like particles is significantly higher than that of polyhedral particles. This phenomenon might be related to the specific surface area of sample. To test this conjecture, the oxygen content per unit surface was calculated according to Eq. (7) [9] (where S_O is oxygen content per unit surface, S_g is specific surface area, and $w_O\%$ is oxygen content).

$$S_O = \frac{w_O\%}{S_g \bullet 100} \tag{7}$$

The S_O values of the two samples are very similar, that is, the O contents of the samples was indeed related to the specific surface area. It could be considered that the oxygen of the ZrB_2 powder was concentrated on the surface of the particles. Since the boronation process was carried out in a sufficient Ca melt, strong reducing effect of Ca did not cause differences in oxygen content between two samples. Because ZrB_2 could be corroded in acidic solution [26, 27], it might be oxidized during acid leaching or drying process. The larger specific surface area would provide a larger interface for the oxidation reaction.

If the total oxygen content of the powder ($\omega_O\%$) was completely concentrated in a thin layer of ZrO_2 (monoclinal) on the surface of spherical product particles, the relationship between particle diameter and oxygen content could be expressed as Eq. (8) (where $\omega_O\%$ is oxygen content of the powder; ρ_{ZrO_2} is density of monoclinal ZrO_2, 5.823 g·cm^{-3}; ρ_{ZrB_2} is density of ZrB_2, 6.118 g·cm^{-3}; D is particle diameter, and equals to D_E; $D_{O\text{-}B}$ is diameter of unoxidized inner ZrB_2 core; M_O is molar mass of oxygen, 16 g·mol^{-1}; M_{ZrO_2} is molar mass of ZrO_2, 123.22 g·mol^{-1}). The thickness of surface oxide layer (d) is given by Eq. (9). The calculation result suggests that the oxide film thicknesses of the two samples are 1.16 nm (cauliflower-like particle) and 1.05 nm (smooth polyhedron), which are close to prepared ZrB_2 particles in literature [14, 24].

$$\frac{\omega_O\%}{100} = \frac{\rho_{ZrO2}\left(D^3 - D_{B-O}^3\right)\frac{2M_O}{M_{ZrO_2}}}{\rho_{ZrB_2}D_{B-O}^3 + \rho_{ZrO_2}\left(D^3 - D_{B-O}^3\right)} \tag{8}$$

$$d = \frac{D - D_{B-O}}{2} \tag{9}$$

Formation mechanism of nano-ZrB_2

To explain the formation of nano-ZrB_2 particles, the mechanism of particle evolution is shown in Fig. 9. In Fig. 9a, the raw material for carbothermal reduction is a mixture of nano-ZrO_2 and carbon black. During the heating process, the ZrO_2 particles will first grow to ~ 200 nm through sintering before the carbothermal reduction reaction begins (below 1330 K). This is because the sintering of nano-ZrO_2 can be performed at a lower temperature (1273 ~ 1473 K). With the further increase of temperature, the carbothermal reduction reaction of ZrO_2 occur, and a new phase ZrC is formed. However, since the growth of ZrC by sintering can only be carried out above 2000 K, the formed ZrC particles will maintain the size of ZrO_2 particles (~ 200 nm). In boronation stage, ZrC is boronized to form ZrB_2 by B_4C in Ca melt. At a low temperature (1373 K, Fig. 9b), since the molar volume of ZrB_2 is larger than that of ZrC, the particle size of boronized product is also larger than that of ZrC. The expansion stress occurred during boriding process may cause the particles to be cauliflower-like. Moreover, each ZrC particle may have multiple nucleation points during boronation reaction, which also lead to that the boronized product appears as cauliflower-like agglomerated particles. Although the size of the agglomerate is ~ 200 nm, the grain size is only tens of nanometers. This cauliflower-like feature is retained because ZrB_2 particles are difficult to grow at lower temperatures. At a higher temperature (1473 K, Fig. 9c), the cauliflower-like particles are no longer stable. ZrB_2 grains will continue to grow to about ~ 100 nm due to the ripening. In addition, the particle shows a smooth polyhedral shape, which is a lower-energy state. In this process, the original agglomerates are also disintegrated, and the dispersity of ZrB_2 powder is also improved. Although the product obtained at 1473 K is resulted from effects of ripeness and growth, the decline of surface of product will effectively decrease the oxygen content of powder product. After comparing the methods in Table 1, the advantages of this method were more obvious. The raw materials used in this process were cheap and easily available, and the reaction could be realized by using an ordinary high-temperature furnace.

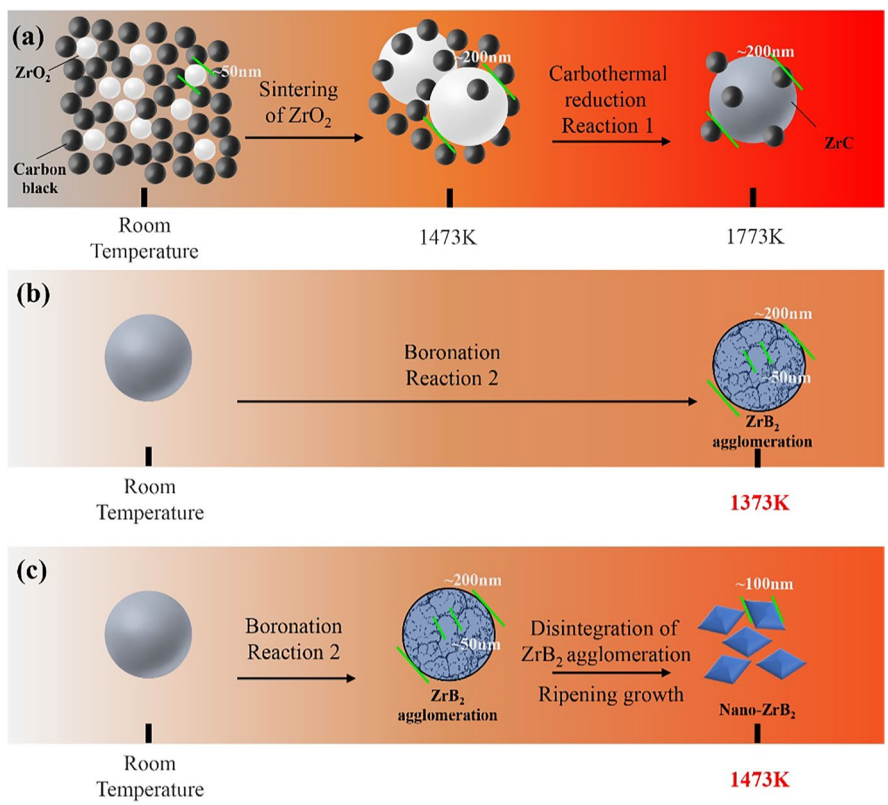

Fig. 9 Formation mechanism of nano-ZrB_2 particles: **a** carbothermal reduction, **b** boronation at 1373 K, **c** boronation at 1473 K

In addition, the product was pure ZrB_2 with particle size of less than 100 nm.

Conclusions

IN this paper, a two-step method of synthesizing nano-ZrB_2 powder was studied in detail. In first stage, fine ZrC was prepared via vacuum reduction of nano-ZrO_2 with carbon black. Next, ZrC was boronized to ZrB_2 by B_4C in Ca melt. Finally, pure phase ZrB_2 was obtained after acid leaching. In carbothermal reduction stage, the carbon proportion was the key factor affecting particle size and uniformity of final ZrB_2. Excess carbon could significantly reduce the large-sized ZrO_2, and ensure the fine size and uniformity of the boronation product. In boronation stage, temperature played an important role in the microstructure of ZrB_2. Cauliflower-like aggregate (~200 nm) and smooth polyhedron (~100 nm) were obtained by boronizing the carbothermal reduced product at 1373 K and 1273 K, respectively. The grain sizes estimated by Scherrer's formula and equivalent particle sizes calculated by BET results of these two products were both less than 100 nm. The formation of nano polyhedral particle with smooth surface was caused by the growth and disintegration of the cauliflower-like agglomerates by ripening at higher temperature. Oxygen analysis results indicated that O element was enriched on the particle surface, and the oxide layer thickness was estimated to be 1.8 nm.

Funding This work was financially supported by the State Key Laboratory of Advanced Metallurgy, University of Science and Technology Beijing, China.

Declarations

Conflict of interest The authors declare no competing interests.

References

1. Fahrenholtz WG, Wuchina EJ, Lee WE, Zhou YC (2014) Ultra-high temperature ceramics: materials for extreme environment applications. John Wiley & Sons, New York
2. Yang X, Wei L, Song W, Bi FZ, Zhao HC (2013) ZrB_2/SiC as a protective coating for C/SiC composites: effect of high temperature oxidation on mechanical properties and anti-ablation property. Compos Part B-Eng 45:1391–1396
3. Zhang YL, Fei T, Zeng WY, Yang BX, Li HJ, Li KZ (2015) Microstructure and oxidation behavior of C/C-ZrB_2-SiC composites coated with SiC coating at high temperature. Corros Sci 100:421–427
4. Chamberlain AL, Fahrenholtz WG, Hilmas GE (2010) Low-temperature densification of zirconium diboride ceramics by reactive hot pressing. J Am Ceram Soc 89:3638–3645
5. Sengupta P, Sahoo SS, Bhattacharjee A, Basu S, Manna I (2021) Effect of TiC addition on structure and properties of spark plasma sintered ZrB_2-SiC-TiC ultrahigh temperature ceramic composite. J Alloy Compd 850:156668
6. Sharma A, Karunakar DB (2021) Effect of SiC and TiC addition on microstructural and mechanical characteristics of microwave sintered ZrB_2 based hybrid composites. Ceram Int 47:26455–26464
7. Zhang D, Hu P, Dong S, Fang C, Feng J, Zhang X (2019) Microstructures and mechanical properties of Cf/ZrB_2-SiC composite fabricated by nano slurry brushing combined with low-temperature hot pressing. J Alloy Compd 789:755–761
8. Zhang D, Feng J, Hu P, Xun L, Liu M, Dong S, Zhang X (2020) Enhanced mechanical properties and thermal shock resistance of C_f/ZrB_2-SiC composite via an efficient slurry injection combined with vibration-assisted vacuum infiltration. J Eur Ceram Soc 40:5059–5066
9. Guo S, Hu C, Kagawa Y (2011) Mechanochemical processing of nanocrystalline zirconium diboride powder. J Am Ceram Soc 94:3643–3647
10. Wu WW, Zhang GJ, Sakka Y (2013) Nanocrystalline ZrB_2 powders prepared by mechanical alloying. J Asian Ceram Soc 1:304–307
11. Jalaly M, Bafghi MS, Tamizifar M, Gotor FJ (2014) An investigation on the formation mechanism of nano ZrB_2 powder by a magnesiothermic reaction. J Alloy Compd 588:36–41
12. Yuan L, Wang C, Bi M, Ma S, Weng (2019) X Effect of processing parameters on the formation process of nano-sized ZrB_2 powders by the high energy ball milling. Adv Appl Ceram 118:395–402
13. Bai L, Jin H, Lu C, Yuan F, Huang S, Li J (2015) RF thermal plasma-assisted metallothermic synthesis of ultrafine ZrB_2 powders. Ceram Int 41:7312–7317
14. Zoli L, Costa AL, Sciti D (2015) Synthesis of nanosized zirconium diboride powder via oxide-borohydride solid-state reaction. Scripta Mater 109:100–103
15. Camurlu HE, Maglia F (2009) Preparation of nano-size ZrB_2 powder by self-propagating high-temperature synthesis. J Eur Ceram Soc 29:1501–1506
16. Wang Y, Wu YD, Peng B, Wu KH, Zhang GH (2021) A universal method for the synthesis of refractory metal diborides. Ceram Int 47:14107–14114
17. Wang Y, Zhang GH, Chou KC (2022) Preparation and oxidation characteristics of ZrC-ZrB_2 composite powders with different proportions. Int J Min Met Mater 29:521–528
18. Rankin J, Sheldon BW (1995) In situ TEM sintering of nano-sized ZrO_2 particles. Mat Sci Eng A 204:48–53
19. Srdić VV, Winterer M, Hahn H (2000) Sintering behavior of nanocrystalline zirconia prepared by chemical vapor synthesis. J Am Ceram Soc 83:729–736

20. Feng L, Lee S, Lee H (2017) Nano-sized zirconium carbide powder: synthesis and densification using a spark plasma sintering apparatus. Int J Refract Met H 64:98–105
21. Núñez-González B, Ortiz AL, Guiberteau F (2012) Nygren M Improvement of the spark-plasma-sintering kinetics of ZrC by high-energy ball-milling. J Am Ceram Soc 95:453–456
22. Wang Y, Zhang GH, Wu YD, He XB (2020) Preparation of CaB_6 powder via calciothermic reduction of boron carbide. Int J Min Met Mater 27:37–45
23. Patterson AL (1939) The Scherrer formula for X-ray particle size determination. Phys Rev 56:978
24. Dilmi N, Bacha NE, Younes A (2020) Structural and magnetic properties of $Fe_{60-x}Ni_x$ $(ZnO)_{40}$ nanocomposites produced by mechanical milling and coated by thermal spraying on a steel substrate. Powder Metall Met Ceram 59:35–45
25. Ortiz AL, Zamora V, Rodríguez-Rojas F (2012) A study of the oxidation of ZrB_2 powders during high-energy ball-milling in air. Ceram Int 38:2857–2863
26. Liu HT, Qiu HY, Guo WM, Zou J, Zhang GJ (2015) Synthesis of rod-like ZrB_2 powders. Adv Appl Ceram 114:418–422
27. Weimer AW (2012) Carbide, nitride and boride materials synthesis and processing. Springer Science & Business Media, Berlin

Publisher's note Springer Nature remains neutral with regard to jurisdictional claims in published maps and institutional affiliations.

Springer Nature or its licensor (e.g. a society or other partner) holds exclusive rights to this article under a publishing agreement with the author(s) or other rightsholder(s); author self-archiving of the accepted manuscript version of this article is solely governed by the terms of such publishing agreement and applicable law.